HAL open science

Galvanic effects induced by siderite and cementite surface layers on carbon steel in aqueous CO2 environments

Joshua Owen, Francois Ropital, Gaurav R. Joshi, Jean Kittel, Richard Barker

To cite this version:

Joshua Owen, Francois Ropital, Gaurav R. Joshi, Jean Kittel, Richard Barker. Galvanic effects induced by siderite and cementite surface layers on carbon steel in aqueous CO2 environments. Corrosion Science, 2022, 209 (110762), 10.1016/j.corsci.2022.110762 . hal-03909974

HAL Id: hal-03909974

https://ifp.hal.science/hal-03909974v1

Submitted on 21 Dec 2022

HAL is a multi-disciplinary open access archive for the deposit and dissemination of scientific research documents, whether they are published or not. The documents may come from teaching and research institutions in France or abroad, or from public or private research centers.

L'archive ouverte pluridisciplinaire **HAL**, est destinée au dépôt et à la diffusion de documents scientifiques de niveau recherche, publiés ou non, émanant des établissements d'enseignement et de recherche français ou étrangers, des laboratoires publics ou privés.

Distributed under a Creative Commons Attribution 4.0 International License

Corrosion Science 209 (2022) 110762

Contents lists available at ScienceDirect

Corrosion Science

journal homepage: www.elsevier.com/locate/corsci

Galvanic effects induced by siderite and cementite surface layers on carbon steel in aqueous CO_2 environments

Joshua Owen [a,*], Francois Ropital [b,c], Gaurav R. Joshi [b], Jean Kittel [b], Richard Barker [a]

[a] Institute of Functional Surfaces, School of Mechanical Engineering, University of Leeds, Leeds LS2 9JT, United Kingdom
[b] IFP Energies Nouvelles, Rond-point de l'échangeur de Solaize, BP 3, 69360 Solaize, France
[c] Univ. Lyon, INSA-LYON, MATEIS UMR CNRS 5510, 69621 Villeurbanne Cedex, France

ARTICLE INFO

Keywords:
Carbon steel
Iron carbide
Iron carbonate
Galvanic corrosion
Localised corrosion
Electrochemistry

ABSTRACT

Siderite ($FeCO_3$) and cementite (Fe_3C) layers develop naturally on carbon steel surfaces in aqueous carbon dioxide (CO_2) environments. This study evaluates galvanic corrosion induced by such layers when coupled to bare carbon steel. In CO_2-saturated, 50 °C, pH 5 conditions, the Fe_3C-filmed carbon steel acted as the net cathode, significantly enhancing bare steel corrosion rates. Galvanic currents induced by the $FeCO_3$-filmed steel were much lower, with $FeCO_3$ removed from the surface as Fe_3C was revealed concomitantly on bare steel. It is proposed that the presence of Fe_3C amongst the $FeCO_3$ layer is responsible for galvanic interaction, rather than $FeCO_3$ itself.

1. Introduction

Carbon steel is widely used as a material for infrastructure in the geothermal, carbon abatement and oil and gas sectors, which can all have environments where the presence of aqueous carbon dioxide (CO_2) creates conditions favourable for corrosion. Dependent on the solution chemistry, numerous naturally occurring layers can form on carbon steel surfaces as they corrode in the mildly acidic CO_2 environments. One such layer is iron carbonate ($FeCO_3$), also known as siderite, a crystalline inorganic mineral with corrosion protective properties when formed under a specific range of aqueous CO_2 conditions [1–10]. Another layer, or more strictly a network, commonly found on corroding carbon steel surfaces is iron carbide (Fe_3C), or cementite, which is revealed as the ferrite phase in the steel preferentially corrodes, leaving the microstructure's carbon-containing phase at the surface [11,12]. Fe_3C is generally associated with enhancing corrosion rates of carbon steel, due its electrically conductive properties (reported electrical resistivity values of 10^{-5} - 10^{-4} Ω•cm across a range of temperatures up to 100 °C [13–15]) and ability to establish a galvanic couple with the bare carbon steel surface [2,11,16–18]. Whereas $FeCO_3$ is often noted for its ability to protect carbon steel and reduce corrosion rates. Localised corrosion, however, can be initiated if the carbon steel surface is only partially covered by $FeCO_3$ [19,20]. Certain studies have suggested that galvanic corrosion between $FeCO_3$ and carbon steel has caused localised corrosion, with the $FeCO_3$ layered regions acting as cathodes and bare steel regions acting as anodes [2,19,21]. However, the role of $FeCO_3$ in galvanic corrosion is more complex, as $FeCO_3$ is an electrical insulator [12,22], with a reported resistivity in the range of 10^3 – 10^5 Ω•cm at 80 °C [23]. Alternative mechanisms have been proposed, whereby galvanic interaction is initiated as a result of local differences in occluded electrolyte chemistry (e.g. pH, Fe^{2+} concentration) underneath $FeCO_3$ crystals and uncovered regions of the steel surface, in a manner similar to under deposit corrosion [6]. Higher local surface pH (compared to bulk solution pH) has also been suggested to initiate pseudo-passivation effects, whereby the carbon steel's open circuit potential (OCP) can increase dramatically during the $FeCO_3$ layer growth process, often observed with the simultaneous formation of other surface layers, such as magnetite [24–26]. This increase in OCP has also been suggested as a cause of galvanic corrosion, with the surface layers formed acting as the net cathode [27].

For galvanic corrosion (and hence localised corrosion in this context) to proceed on carbon steel, in the presence of a surface layer, exposure of the bare steel and/or the region under the surface layer to the electrolyte is essential. The layered region typically acts as the net cathode and the bare steel acts as the net anode, accelerating dissolution of the bare steel [2,19,21]. In a CO_2 environment, the cathodic and anodic reactions proceed after CO_2 dissolves in water to form carbonic acid, which then partially dissociates to provide a source of hydrogen ions (H^+). The

* Corresponding author.
E-mail address: J.J.Owen@leeds.ac.uk (J. Owen).

https://doi.org/10.1016/j.corsci.2022.110762
Received 28 June 2022; Received in revised form 6 October 2022; Accepted 18 October 2022
Available online 20 October 2022
0010-938X/© 2022 The Authors. Published by Elsevier Ltd. This is an open access article under the CC BY license (http://creativecommons.org/licenses/by/4.0/).

cathodic reaction is the evolution of H_2 through proton reduction at the carbon steel surface:

$$2H^{+}_{(aq)} + 2e^{-} \rightarrow H_{2(g)} \quad (1)$$

The anodic dissolution of iron is summarised by the following equation:

$$Fe_{(s)} \rightarrow Fe^{2+}_{(aq)} + 2e^{-} \quad (2)$$

The role of Fe_3C in carbon steel corrosion has been widely been discussed, with the layer playing a critical role in enhancing the corrosion rate of carbon steel as it corrodes, due to the galvanic interaction between the layer and the bare steel surface [11,12,18,28,29]. Fe_3C has been shown to act as the net cathode when a conductive pathway is established with carbon steel [2]. Experimentally, gradual increases in uniform corrosion rates of carbon steel are attributed to revealing of the Fe_3C network on the surface [11,30]. Another theory proposed for the increase in corrosion rates, in the presence of an undissolved Fe_3C network layer, is that of acidification within the Fe_3C network [12,16]. Highly porous structures, favourable for local acidification, are observed when an Fe_3C network is revealed on the carbon steel surface [11,28].

Concerning the galvanic interaction initiated by $FeCO_3$, research has generally focused on environments where protective layers do not fully form on the surface. In conditions close to the saturation point of $FeCO_3$, where the rate of growth would be considerably slower than in supersaturated conditions, localised corrosion of carbon steel has been observed [19]. However, when only partial coverage of the surface is achieved, for example, after removal or dissolution of the $FeCO_3$ layer [7,17,20,31] or when conditions are not favourable for sufficient $FeCO_3$ growth to cover the surface [3,32], bare regions of the steel remain exposed to electrolyte. Despite having electrically insulating properties, galvanic currents between $FeCO_3$-covered carbon steel and bare carbon steel have been recorded [2,19,21].

To investigate galvanic interaction between bare steel and $FeCO_3$, Han et al. [19] utilised an artificial pit technique consisting of a retracted carbon steel coupon (acting as the net anode) surrounded by a significantly larger surface area carbon steel coupon (acting as the net cathode), at a net cathode to net anode area ratio (AR) of 1000:1. For the purpose of their galvanic corrosion experiments, the pit depth utilised was < 0.1 mm. The cathode coupon surface layer was initially exposed to a pH 6.6, aqueous CO_2 solution at 80 °C to form an $FeCO_3$ layer, before pH was dropped to approximately pH 5.8 and the bare net anode steel coupon was immersed in the solution. The two coupons were externally coupled using a zero-resistance ammeter (ZRA) and a galvanic current was measured between the $FeCO_3$-layered coupon (net cathode) and bare carbon steel (net anode) in the lower pH environment. Fernandez et al. [21] performed galvanic corrosion experiments by coupling a steel coupon covered with an $FeCO_3$ layer to a bare carbon steel coupon at ARs of 1, 50, 100 and 200:1. The galvanic interaction was not significant at an AR of 1:1, but was considerably higher at the other ARs, of the order of 10^{-4} A/cm^2. Barker et al. [2] developed an abrasion rig capable of removing surface layers from a carbon steel pin, which was coupled using a ZRA to a larger surface area carbon steel coupon at an AR of ~150:1. Galvanic interaction of both Fe_3C and $FeCO_3$ layers was evaluated, with the pin coupon periodically abraded to remove the layer. Galvanic interaction was observed after the layer removal, with the magnitude of galvanic current greater as the experiment progressed and the layer became more established. In each of these studies, the driving force for the galvanic interaction has been attributed to the difference in OCP between the net cathode and net anode.

One key parameter not considered in these studies was the presence of the more electrically conductive Fe_3C on the $FeCO_3$-layered coupons, and the influence this has on galvanic corrosion. Numerous authors have reported the presence of Fe_3C in addition to the $FeCO_3$ layer [1,9,11,12,31,33] on carbon steel surfaces. Galvanic currents were higher for Fe_3C-bare steel couples compared to $FeCO_3$-bare steel couples in the study by Barker et al. [2], albeit in different conditions so a direct comparison could not be made. Therefore, the question remains as to whether the $FeCO_3$ itself causes the galvanic interaction, or if it is in fact caused by the presence of Fe_3C within the $FeCO_3$ layer. To establish a thorough understanding of the role of Fe_3C and $FeCO_3$ layers on the galvanic corrosion of bare carbon steel in this study, Fe_3C and $FeCO_3$ layered coupons were galvanically coupled to bare carbon steel in the same aqueous CO_2-saturated conditions. The application of electrochemical and surface analysis techniques enabled the effects of galvanic corrosion to be characterised and quantified.

2. Experimental procedure

2.1. Material preparation

X65 carbon steel was used as the test material for most experiments. Coupons were machined into 6 mm thick discs, with diameters of 25 mm (giving a surface area 4.9 cm^2) and 7.9 mm (surface area of 0.49 cm^2). X65 steel has a ferritic-pearlitic microstructure with the chemical composition (wt%) of Fe (97.8), C (0.15), Mn (1.42), Ni (0.09), Nb (0.054), Mo (0.17), Si (0.22), V (0.06), P (0.025) and S (0.02). After etching in 2% Nital solution, the ferritic-pearlitic microstructure of X65 carbon steel was observed using a light microscope image, shown in Fig. S1 in the Supplementary Material. Pure iron (>99.8%) coupons (6 mm thick discs, 7.9 mm diameter) were also used for comparison. To facilitate electrochemical measurements, an insulated copper wire was soldered to the reverse side of a coupon before it was embedded in a non-conductive epoxy resin. The coupons were then wet ground up to 1200 grit (depending on the experiment) using silicon carbide (SiC) grinding paper, degreased with acetone, rinsed with deionised water, and dried with compressed air. All sample preparation was performed within 30 min of starting an experiment.

2.2. Solution preparation

All corrosion experiments were performed in CO_2-saturated, sodium chloride (NaCl) solutions, with details of each experiment's conditions provided in the following sections. Analytical grade NaCl (Sigma) was added to 1 L of deionised water, along with analytical grade sodium hydrogen carbonate ($NaHCO_3$, Alfa Aesar), when required, to increase pH. All experiments utilised a glass beaker mounted on a hot plate, as demonstrated in Fig. 1, and gentle stirring of the solution. CO_2 was bubbled into the solution for a minimum of 12 h prior to, and throughout, the experiment to remove dissolved oxygen and fully saturate with CO_2.

2.3. Experimental methods

The two main experiments were categorised as 'surface layer preparation' experiments, in which surface layers were formed in aqueous CO_2 conditions on carbon steel coupons, and 'galvanic corrosion' experiments, where the formed surface layers were coupled to bare coupons.

2.3.1. Method I – Fe_3C network preparation experiments (50 °C, pH 3.8, 1 wt% NaCl, pCO_2 = 0.87 atm, 24 h)

In order to reveal an Fe_3C network on the X65 carbon steel surface, a 1 wt% NaCl solution was prepared in a glass beaker, as demonstrated in Fig. 1. The pH of the solution was not adjusted after CO_2 saturation was achieved, reaching pH 3.8 before the start of experiments (confirmed using a pH probe). These conditions were chosen as no other surface films (i.e. $FeCO_3$) were expected to develop [30]. The solution was heated to a temperature of 50 °C using a thermocouple and temperature controlled hot plate. X65 carbon steel coupons (4.9 cm^2 surface area) were wet ground using 180, 600, 800 and 1200 grit SiC papers prior to the experiment. Two coupons were immersed in the 1 L solution for a

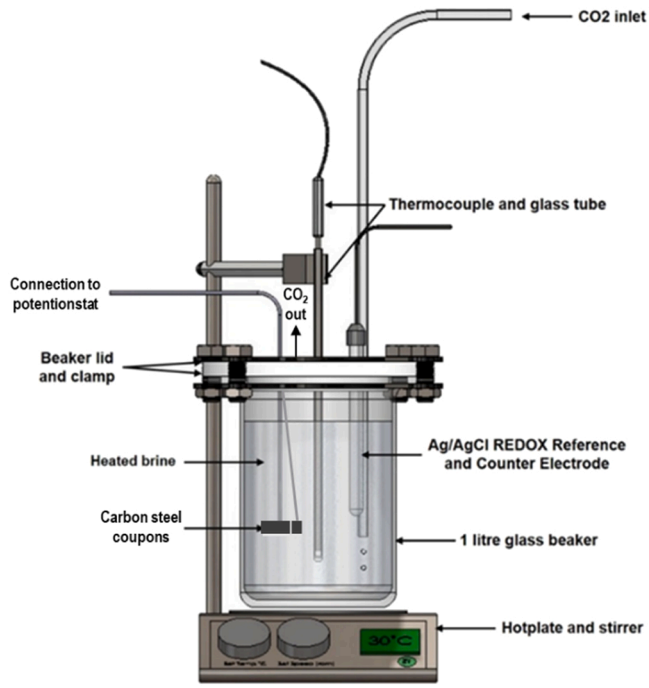

Fig. 1. Glass beaker setup for aqueous CO_2 corrosion experiments. For galvanic corrosion experiments, two coupons were immersed in the solution and coupled using a ZRA.

period of 24 h. Electrochemical measurements were performed in situ to obtain corrosion rates throughout the test period, summarised below.

2.3.2. Method II – $FeCO_3$ layer preparation experiments (80 °C, pH 6.8, 3.5 wt% NaCl, pCO_2 = 0.54 atm, 20 h)

To develop a robust and protective $FeCO_3$ layer on the X65 carbon steel surface, a 3.5 wt% NaCl solution was prepared in a glass beaker and heated to 80 °C, as demonstrated in Fig. 1. The pH of the solution was adjusted to pH 6.8 using $NaHCO_3$. These conditions were chosen as protective $FeCO_3$ layers have been shown to form on carbon steel in this environment previously, with thorough characterisation of the layers performed using XRD and electrochemical techniques [3,4,6]. X65 carbon steel coupons were wet ground progressively using 180, 400 and 600 grit SiC grinding papers prior to starting the experiment, with a rougher surface preferred for these experiments (compared to Fe_3C layer growth experiments) to promote sites for nucleation of $FeCO_3$ crystals [34]. Two coupons were immersed in solution for a period of 20 h, with this time sufficient to achieve extensive coverage of the layer on the surface [3], whilst being short enough to avoid inducing pseudo-passivation effects and the formation of magnetite, a semi-conductor which readily establishes a galvanic couple with carbon steel [15,35]. Magnetite has been observed in similar environments after a number of days of exposure [5,36]. Electrochemical measurements were performed in situ to obtain corrosion rates throughout the 20 h test period.

2.3.3. Method III - control experiments (50 °C, pH 5, 1 wt% NaCl, pCO_2 = 0.87 atm, 24 h)

For galvanic corrosion measurements, a 1 wt% NaCl solution was prepared in the glass beaker configuration shown in Fig. 1. The solution was heated to 50 °C and adjusted to pH 5 using $NaHCO_3$. To elucidate the difference between uniform and galvanic corrosion effects, experiments were initially performed in the absence of galvanic coupling, acting as control results. These experiments were carried out using both bare (i.e. immediately after being wet ground prior to the experiment using 180, 600, 800 and 1200 grit SiC grinding paper) X65 steel coupons and layered coupons, transferred immediately to the pH 5 solution after Method I and Method II experiments. One coupon was immersed in the solution per experiment. All experiments were performed over a period of 24 h, with in situ electrochemical techniques utilised to determine corrosion rates.

These conditions enabled the effects of both Fe_3C and $FeCO_3$ covered steel surfaces to be directly compared when galvanically coupled to bare carbon steel, without significant changes to the properties of the layers induced by the environment of exposure. Due to the dynamic properties of the surface and localised nature of galvanic corrosion, identifying controllable and representative conditions is challenging. Localised variations near the steel surface, which could influence galvanic corrosion, such as interfacial pH changes [25], acidification within the Fe_3C structure [16] and heterogeneity in carbon steel microstructure and layer characteristics [34], are difficult to replicate. Previous studies which evaluated galvanic interaction of these layers have either been undertaken in the conditions in which the layer formed [2,21] or in conditions close to the saturation point of $FeCO_3$, thus replicating conditions in which localised corrosion may be expected (i.e. conditions most likely to result in partial coverage), after pre-forming the layers in supersaturated conditions [19]. However, in those experiments, conditions have favoured either $FeCO_3$ or Fe_3C growth, making a direct comparison between the galvanic corrosion caused by each layer difficult. In conditions close to the saturation point, significant decreases in carbon steel corrosion rate have still been observed due to $FeCO_3$ crystal growth [5]. At pH 5, corrosion rates were expected to be lower than at pH 3.8, thus reducing the rate at which Fe_3C would be revealed. In pH 5 conditions at a temperature of 50 °C, further growth of $FeCO_3$ layers would be limited, whilst dissolution of $FeCO_3$ on layered coupons would also be minimised, which would be excessive at pH < 5 [1]. Carrying out such control experiments enabled a clear distinction between galvanic corrosion and other associated effects (e.g. dissolution of $FeCO_3$ in the under-saturated environment) to be identified.

2.3.4. Method IV – Galvanic corrosion measurements (50 °C, pH 5, 1 wt% NaCl, pCO_2 = 0.87 atm, 4 h and 24 h)

In galvanic corrosion measurements, a layered coupon was removed from the solution at the end of the Method I/Method II layer preparation experiments, dried using a heat gun (as opposed to compressed air, which could potentially damage the layers) and immediately immersed in the pH 5 solution, along with a bare X65 steel coupon (wet ground with 1200 grit SiC paper). The two coupons were immersed into the solution at the same height adjacent to each other, to minimise ohmic drop, and galvanically coupled externally using a ZRA for a period of 4 h and 24 h. The surface area of the bare steel coupon (net anode) used was either 4.9 cm^2, to give an AR of 1:1, or 0.49 cm^2, giving an AR of 10:1. It is noted that the electrochemically active surface area of the net cathode would be somewhat different once the surface layer has been prepared. However, exact quantification of this surface area is not possible in this context so surface area is reported as the coupon geometrical surface area. Significantly higher ARs in studies of similar layers, such as 50–200:1 [21], 150:1 [2] and 1000:1 [19], have demonstrated that galvanic currents are observed when coupled to bare carbon steel. However, these ARs may not be representative of partial layer coverage. Lazareva et al. [6], Al Kindi et al. [37] and De Motte et al. [5] reported, after implementation of electrochemical impedance spectroscopy (EIS), that the true actively corroding surface area (i.e. regions of carbon steel not blocked by $FeCO_3$) ranged from 10% to 50% of the original coupon surface area, even when corrosion rates were reduced significantly by the $FeCO_3$ layer. Therefore, it was felt by the authors that lower ARs were most representative of the application of interest. Additional experiments were performed by coupling an $FeCO_3$-layered coupon to a pure iron coupon, at an AR of 10, using the same methodology.

2.4. Electrochemical measurements

2.4.1. Linear polarisation resistance measurements

Linear polarisation resistance (LPR) measurements were performed in situ during the layer preparation and control experiments (Methods I, II and III). The carbon steel coupons were used as the working electrode, with a combination silver/silver chloride (Ag/AgCl) and platinum (Pt) counter electrode used to complete the three-electrode cell. The working electrode was polarised from − 15 mV to + 15 mV relative to OCP at a scan rate of 0.25 mV/s. LPR measurements were performed every 15 min for the entire experimental period, with OCP monitored in between. To determine the corrosion rate (V_c) in mm/year from LPR measurements, polarisation resistances (R_p) were corrected to account for solution resistance (R_s), enabling the determination of charge transfer resistances ($R_{ct} = R_p - R_s$) in Ω·cm^2. Corrosion current density (i_{corr}) in A/cm^2 could then be calculated, Eq. (3).

$$i_{corr} = \frac{B}{R_{ct}} = \frac{1}{R_{ct}} \frac{\beta_a \beta_c}{2.303(\beta_a + \beta_c)} \tag{3}$$

where B is the Stern-Geary coefficient (V/decade), β_a is the anodic Tafel constant (V/decade) and β_c is the cathodic Tafel constant (V/decade). Once a corrosion current density was obtained, the corrosion rate could be calculated:

$$V_c = \frac{K i_{corr} M_{Fe}}{nF\rho} \tag{4}$$

where K is a constant to convert the corrosion rate into mm/yr ($K = 3.16 \times 10^8$), M_{Fe} is the molecular mass of iron (55.8 g/mol), n is the number of electrons liberated in the anodic reaction ($n = 2$), F is Faraday's constant (96,486 C/mol) and ρ is the density of the steel (7.87 g/cm^3).

2.4.2. Electrochemical impedance spectroscopy measurements

EIS measurements were performed on the carbon steel working electrode over a frequency range from 20,000–0.1 Hz at an amplitude of ± 10 mV vs. OCP. For each frequency decade, 10 measurements were carried out. Measurements were performed 5 min after immersing an X65 carbon steel coupon (4.9 cm^2 surface area) in solution in the pH 3.8, pH 5 and pH 6.8 conditions. From EIS measurements, solution resistance was determined as the high frequency limit of the real part of the impedance. To account for minor differences in the positioning of large and small surface area coupons within the beaker, additional EIS measurements were performed using a 0.49 cm^2 X65 steel coupon. Solution resistances for the 4.9 cm^2 coupons of 35.7 Ω•cm^2 (pH 3.8), 34.6 Ω•cm^2 (pH 5) and 6.33 Ω•cm^2 (pH 6.8), were obtained, with a value of 12.4 Ω•cm^2 measured using the 0.49 cm^2 in pH 5, 50 °C, 1 wt% NaCl conditions. These values of solution resistance were then used for ohmic drop compensation of potentiodynamic polarisation and LPR measurements. Nyquist plots are provided in the Supplementary Material.

2.4.3. Potentiodynamic polarisation measurements

Potentiodynamic polarisation measurements were carried out at the end of the experiment to obtain Stern-Geary coefficients and thus calculate corrosion rates, using Eqs. (3) and (4). Additional potentiodynamic polarisation measurements were performed 15 min after immersing coupons in the 1 wt% NaCl, pH 5, 50 °C solution (Method III). Cathodic kinetics were measured first, polarising the working electrode from + 5 to − 250 mV vs OCP at a scan rate of 0.5 mV/s, followed by anodic polarisation from − 5 to + 250 mV vs OCP at a scan rate of 0.5 mV/s. A 4 min period in between the cathodic and anodic measurements without polarisation allowed OCP to stabilise. Results were corrected for ohmic drop to account for solution resistance using the values reported in Section 2.4.2. Polarisation significantly beyond OCP (>> ± 15 mV) can fundamentally change the nature of surface layers that form (or have formed) on carbon steel [34]. For this reason, potentiodynamic polarisation measurements were completed as the final measurement in an experiment and coupons were not used in any further analysis or experiments. However, potentiodynamic polarisation measurements are widely used to evaluate $FeCO_3$ layer behaviour on carbon steel in CO_2 environments [1,3] and were implemented in this study compare the behaviour of different coupons under the same polarisation conditions.

2.4.4. Zero Resistance Ammeter (ZRA) measurements

Coupons in galvanic corrosion experiments (Method IV) were coupled using a potentiostat and ZRA, enabling the measurement of galvanic current and mixed galvanic potential. Measurements were started immediately after immersing the coupons in the solution and data points were measured every 1 s. Galvanic potential was also monitored during this period using a Ag/AgCl reference electrode.

2.5. Surface analysis

2.5.1. Scanning electron microscopy

Scanning electron microscopy (SEM) imaging was carried out on a Carl Zeiss EVO MA15 SEM to analyse the nature of the X65 carbon steel surfaces (top view) after the different types of solution exposures detailed above. Coupons were removed from the solution at the end of the experiment, removed from the epoxy resin, taking care not to damage the surface or surface layer, and carbon coated from the top surface to the bottom surface to enhance conductivity before mounting on the instrument stage. Images were obtained at an operating voltage of 20 kV in secondary electron mode.

2.5.2. Focused ion beam-scanning electron microscopy

Cross section images of the coupon surface layers after experiments were obtained by milling using a FEI Helios G4 CX DualBeam focused ion beam (FIB)-SEM instrument. Coupons were carbon coated and mounted in the instrument, before orientating at 52° relative to the SEM beam axis and depositing a Pt layer using the gallium ion beam at an operating current of 0.23 nA. Cross sectioning was performed at an operating current of 21 nA, to remove a 15 μm wide x 10 μm deep region from the surface for analysis. A series of cleaning processes then followed using the gallium ion beam at an operating current of 2.5 nA to smooth the texture of the surface for enhanced image quality. SEM images of the cross sections were obtained at an operating voltage of 5 kV in secondary electron mode.

2.5.3. X-ray diffraction analysis

X-ray diffraction (XRD) analysis was undertaken using a Bruker D8 X-ray diffractometer, with a copper (Cu) source, to identify the composition of the surface layers. A 10 × 10 mm region in the centre of the coupons was analysed over a 2θ range from 20° to 70° at a step size 0.032°/second. Additional focused scans from 30° to 45° at a lower step size of 0.016°/second intensified Fe_3C peaks to aid their identification.

3. Results and discussion

3.1. Preparation of layered coupons (Methods I and II)

Corrosion rates measured at pH 3.8 and pH 6.8 are reported in Fig. 2, determined from LPR measurements. The average corrosion rate (with OCP shown in Supplementary Material) is reported from a minimum of three replicate experiments, with error bars representing the standard deviation. To obtain the corrosion rates plotted in Fig. 2, Tafel constants were obtained from the potentiodynamic polarisation plots (see Supplementary Material). A Stern Geary coefficient of 26.0 mV (β_a = 88 mV/decade, β_c = 187 mV/decade) was used to calculate corrosion rates at pH 3.8, based on an average of Tafel constants extracted from three repeat potentiodynamic polarisation plots. A Stern Geary coefficient of 17.4 mV (β_a = 60 mV/decade, β_c = 120 mV/decade) was

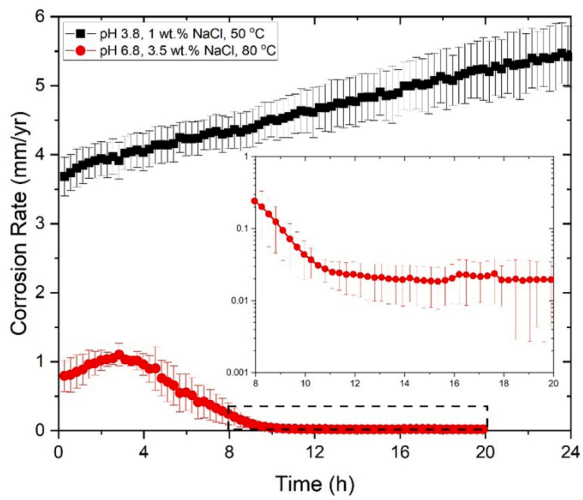

Fig. 2. Corrosion rates, determined from LPR measurements, to establish an Fe_3C network on X65 steel (Method I) in CO_2-saturated, pH 3.8, 1 wt% NaCl conditions at 50 °C and $FeCO_3$ layers on X65 steel (Method II) in CO_2-saturated, pH 6.8, 3.5 wt% NaCl conditions at 80 °C.

utilised at pH 6.8, obtained previously [3].

In pH 3.8 conditions, a gradual increase in corrosion rate from approximately 3.6 mm/yr to 5.5 mm/year was observed over 24 h exposure period, that can be attributed to the revealing of Fe_3C on the carbon steel surface [11]. In pH 6.8 conditions, corrosion rates in Fig. 2 decreased from a maximum value of approximately 1.1 mm/yr to < 0.1 mm/yr as a protective $FeCO_3$ layer formed. An initial increase in corrosion rate was observed during the first 4 h of the experiment, attributed to the revealing of an Fe_3C network before the nucleation and growth of $FeCO_3$ crystals commences [6,9,11], a trend not observed when $FeCO_3$ layers form on pure iron (where Fe_3C is absent) [27,38].

LPR measurements were utilised to demonstrate that a general decreasing corrosion rate trend was observed as $FeCO_3$ layers formed, represented by a significant increase in R_p. However, the authors acknowledge that the accuracy of LPR measurements diminishes for corrosion rate calculation in the presence of a protective surface layer [5,33,37,39]. EIS measurements performed in the same experimental conditions showed a significant increase in charge transfer resistance over the first 20 h of experiment, as the $FeCO_3$ layer formed on the surface [6]. Charge transfer resistances in the range of 1500–2300 $\Omega \bullet cm^2$ were reported after 20 h, a tenfold increase compared to values measured before a layer formed, equivalent to corrosion rates decreasing to < 0.1 mm/yr, in a similar trend to Fig. 2. For the purpose of this study, the general trend of corrosion rate obtained from LPR measurements vs. time is shown, to enable comparisons with experiments performed in different conditions in this study and as reported in the literature when an $FeCO_3$ layer forms [3,19,38].

To identify surface compositions on post-exposure steel surfaces, XRD analyses were carried out. The diffractogram is presented in Fig. 3. Peak assignment was carried out with reference to the International Centre for Diffraction Data (ICDD) references 04–015-6716 ($FeCO_3$) and 00–003–0400 (Fe_3C). Clear $FeCO_3$ peaks are observed on the diffraction pattern associated carbon steel coupon exposed to pH 6.8 conditions (Method II), in addition to the α-Fe planes from the substrate. Some Fe_3C was observed on the $FeCO_3$ coupon, however for clarity this coupon is referred to as the $FeCO_3$-layered coupon throughout. Fe_3C is commonly observed on carbon steel coupons when $FeCO_3$ forms, playing an intrinsic role in the nucleation and growth of $FeCO_3$ crystals [12]. Due to the relatively low intensity of assigned Fe_3C peaks, an additional scan was carried out in the 30 – 45° 2θ range at a reduced scan step size on the carbon steel coupon exposed to pH 3.8 conditions (Method I), shown in Fig. 3(b). Peaks representing Fe_3C on the coupons exposed to pH 3.8

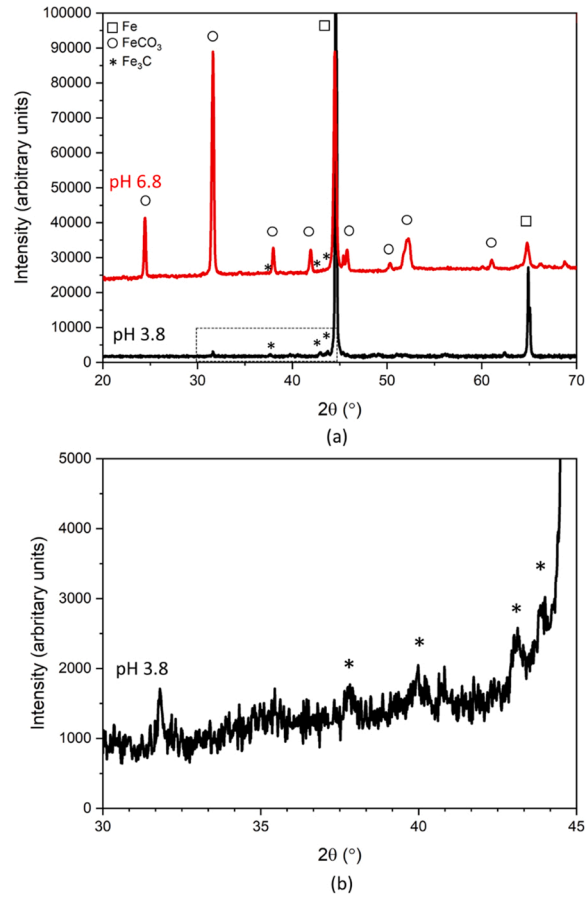

Fig. 3. XRD patterns in (a) a 2θ range from 20° to 70° at a step size of 0.032°/second and (b) a 2θ range from 30° to 45° at a step size of 0.016°/second for an X65 carbon steel coupon after 24 h exposure to pH 3.8 (Fe_3C network, Method I), CO_2-saturated 1 wt% NaCl solution at 50 °C (black line) and carbon steel coupon after 20 h exposure to pH 6.8 ($FeCO_3$ layers, Method II), CO_2-saturated 3.5 wt% NaCl solution at 80 °C (red line). The box in (a) shows the region of the more detailed scan in (b).

were confirmed (Method I). A very low intensity peak at approximately 32° ($FeCO_3$ (104)) was observed, suggesting some $FeCO_3$ was also present at pH 3.8.

Fig. 4 shows SEM and FIB-SEM images of the carbon steel surfaces after exposure to pH 3.8 and pH 6.8 conditions. A porous Fe_3C network (with a thickness of 3.7 ± 1.4 μm) is visible on the surface of the coupon exposed to pH 3.8 solution (Method I), shown in Fig. 4(a) and (c) widely covering the surface. Layers of similar appearance, identified as Fe_3C, have been observed in other studies of carbon steel corrosion [28,40]. The porous structure (observed in the cross-section) and incomplete surface coverage (from the top view image) of the Fe_3C network suggests both pore acidification [16] and galvanic corrosion [11] could be feasible mechanisms leading to enhanced corrosion of carbon steel. $FeCO_3$ crystals are not observed on SEM images in Fig. 4(c), suggesting its presence is negligible.

Fig. 4(b) and (d) show wide coverage of $FeCO_3$ crystals (with the lateral size of the crystal ranging from 8 μm to 22 μm) on the carbon steel surface, explaining the decrease in the corrosion rate observed in Fig. 2. Similar crystals (in terms of size and morphology) were observed and confirmed as $FeCO_3$ in other studies [1,3,5]. The high-resolution cross section in Fig. 4(d) shows a single $FeCO_3$ crystal adhered to the steel surface with an average thickness of 2.5 ± 1.0 μm.

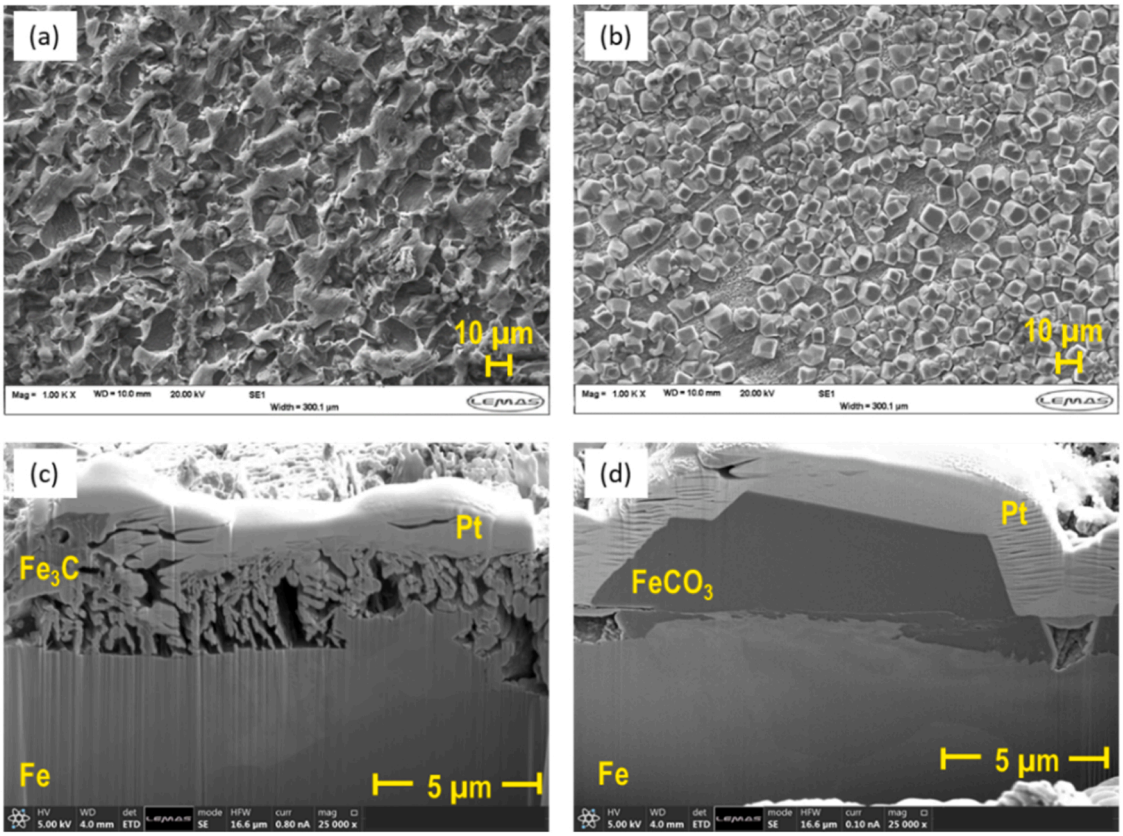

Fig. 4. Top view (a, b) SEM images in secondary electron mode at an operating potential of 20 kV and cross-section (c, d) SEM images in secondary electron mode at an operating potential of 5 kV after FIB milling of (a, c) a carbon steel coupon after 24 h exposure to pH 3.8 (Method I), CO_2-saturated 1 wt% NaCl solution at 50 °C, showing the revealing of an Fe_3C network on the surface and (b, d) a carbon steel coupon after 20 h exposure to pH 6.8 (Method II), CO_2-saturated 3.5 wt% NaCl solution at 80 °C, showing wide coverage of the surface with $FeCO_3$ crystals.

3.2. Control experiments at pH 5 (Method III)

To identify the difference between galvanic corrosion and uniform corrosion in the pH 5, CO_2-saturated, 1 wt% NaCl solution at 50 °C, both blank carbon steel coupons and layered coupons were evaluated in the conditions without galvanic coupling. LPR measurements on each of the different coupons are shown in Fig. 5, converted into corrosion rates over a 24 h period. For the bare carbon steel, a Stern-Geary coefficient of 29.2 mV (β_a = 101 mV/decade, β_c = 199 mV/decade) was obtained from potentiodynamic polarisation measurements, undertaken at the end of the 24 h experiment. The same Stern-Geary coefficients applied in Fig. 2 were once again utilised to calculate corrosion rates, plotted in Fig. 5 for the Fe_3C-layered and $FeCO_3$-layered coupons. The Supplementary Material includes the potentiodynamic polarisation plots for each coupon measured at the end of the 24 h exposure period.

The corrosion rate of the Fe_3C-layered coupon continued to increase throughout the experiment when transferred into the pH 5 solution, suggesting continued revealing of the Fe_3C network. The top view SEM image of this coupon after 24 h exposure to pH 5 solution (Fig. 5(c)) showed that an Fe_3C network remained on the surface. The $FeCO_3$–layered coupon also showed an increase in corrosion rate over the 24 h period. Evidence of $FeCO_3$ dissolution, characterised by reduced surface coverage, reduced crystal size and subtle changes in the shape of crystals [31,41], was observed in pH 5 conditions (i.e. pH below the saturation point of $FeCO_3$ [19]), explaining the increase in corrosion rate observed. However, considerable coverage of $FeCO_3$ remained on the surface, as confirmed by the SEM top-view image in Fig. 5(d). The dissolution of $FeCO_3$ is defined by:

$$FeCO_{3(s)} + H^+_{(aq)} \rightarrow Fe^{2+}_{(aq)} + HCO^-_{3(aq)} \quad (5)$$

where an H^+ ion is consumed during the dissolution process, producing an Fe^{2+} ion and bicarbonate (HCO_3^-) ion.

One key factor that would influence galvanic corrosion studies was that an Fe_3C network unavoidably also formed on the surface of the 'bare steel' coupon. This factor is often not considered in studies of galvanic corrosion between layered coupons and carbon steel in aqueous CO_2 environments. An increase in corrosion rate was measured over 24 h for the bare X65 steel coupon, and the top-view SEM image Fig. 5(b) confirms that Fe_3C was present on the surface. Interestingly, the enhancement in corrosion rate was far greater for the bare steel coupon than the Fe_3C-layered coupon in the pH 5 conditions, with both coupons reaching a similar corrosion rate after 24 h. Therefore, in a galvanic corrosion experiment, the revealing of Fe_3C on the bare steel coupon would generate sites for the cathodic reaction to be supported, changing the condition of the coupled surfaces as the experiment progressed. Despite this, the majority of galvanic corrosion experiments in this study were carried out by coupling the layered coupons to X65 carbon steel, as the authors felt this would be most representative with regards to simulating the scenarios of interest (e.g. partial coverage of layers on a carbon steel surface). Additional experiments were performed by coupling layered coupons to pure iron to evaluate galvanic corrosion using a net anode consisting predominantly of Fe, preventing the formation of Fe_3C on its surface.

To evaluate the corrosion behaviour of the different coupons and identify the initial net cathode and net anode in galvanic corrosion experiments, potentiodynamic polarisation measurements in the pH 5, 1 wt% NaCl solution at 50 °C were carried out 15 min after immersing each coupon (Fe_3C-layered, $FeCO_3$-layered, bare X65 carbon steel, pure iron) in the solution, without galvanic coupling. Fig. 6 showed that initially the layered coupons would act as the net cathodes, due to more

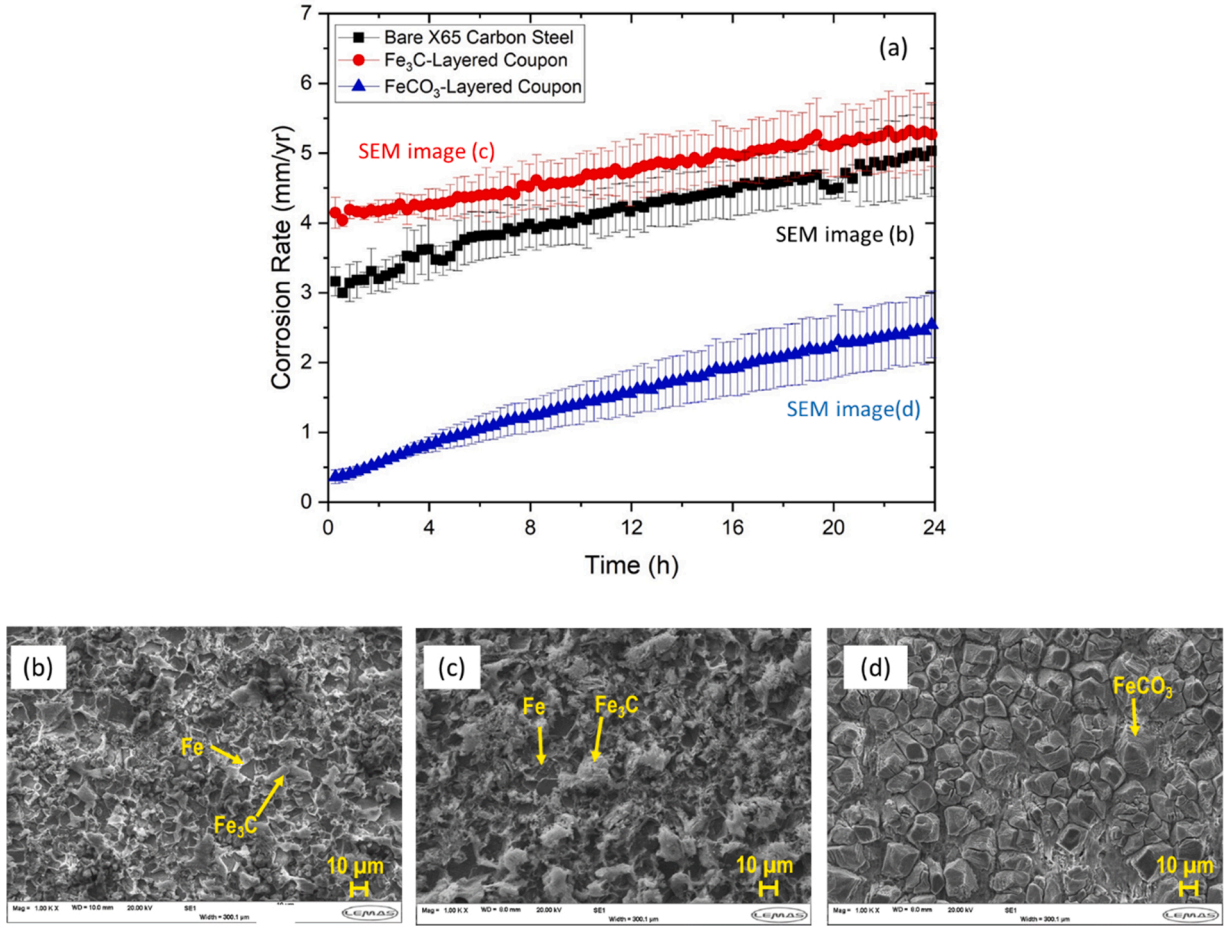

Fig. 5. (a) Corrosion rates, determined from LPR measurements, of bare X65 carbon steel and layered coupons in a CO_2-saturated, pH 5, 1 wt% NaCl solution at 50 °C and top-view SEM images after 24 h exposure of (b) bare X65 steel, (c) an Fe_3C-layered X65 steel coupon and (d) an $FeCO_3$-layered X65 steel coupon.

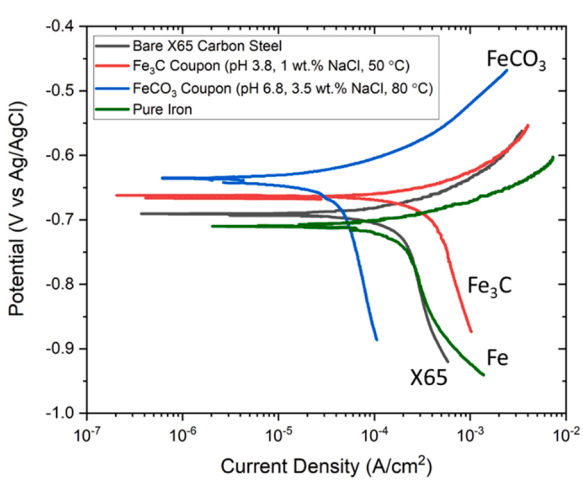

Fig. 6. Potentiodynamic polarisation plots measured after 15 min of immersion in a pH 5, CO_2-saturated 1 wt% NaCl solution at 50 °C of a wet ground X65 carbon steel coupon, a wet ground pure iron coupon, an Fe_3C-layered X65 carbon steel coupon and an $FeCO_3$-layered X65 carbon steel coupon.

a noble OCP compared to bare steel and pure iron, which would perform as the net anodes. The greater corrosion protection provided by the $FeCO_3$ layer on the carbon steel coupon was observable through its lower corrosion current density compared against the other three curves, with this coupon also exhibiting the largest OCP difference compared to bare steel and pure iron.

3.3. Galvanic corrosion experiments (Method IV)

Galvanic corrosion experiments were carried out by immersing layered coupons in the pH 5 solution and coupling them to a 1200 grit SiC wet ground X65 steel coupon. The galvanic currents measured, reported as a current density relative to the bare steel coupon surface area at an AR of 1:1 and 10:1, are presented in Fig. 7. An inset plot focusing on the first 4 h is shown within each 24 h plot. The galvanic potential vs Ag/AgCl is also reported in Fig. 7. Data points were obtained every 1 s, with the markers on the plot representing every 5000th measurement over 24 h and every 1000th measurement over 4 h. The average galvanic current and galvanic potential are reported, obtained from a minimum of three repeat experiments, with error bars showing the standard deviation.

Significantly higher galvanic currents were measured for the Fe_3C-bare X65 steel galvanic couple compared to the $FeCO_3$-bare X65 steel couple. Higher galvanic currents were also measured for the larger AR couples. In Fig. 7(a), for the Fe_3C-bare steel couple, anodic galvanic currents initially started high and decreased rapidly within 1 h, before a more gradual decrease was observed up to, and beyond, 4 h. The galvanic currents remained greater than 0 μA/cm^2 during the first 4 h, stabilising at approximately 0 μA/cm^2 for the remainder of the experiment, thus confirming Fe_3C as having the behaviour of a net cathode. Similar decreasing trends in galvanic current were observed in other studies [2,19,21]. Barker et al. [2] showed that as more Fe_3C was revealed on the carbon steel surface, galvanic interaction with bare steel

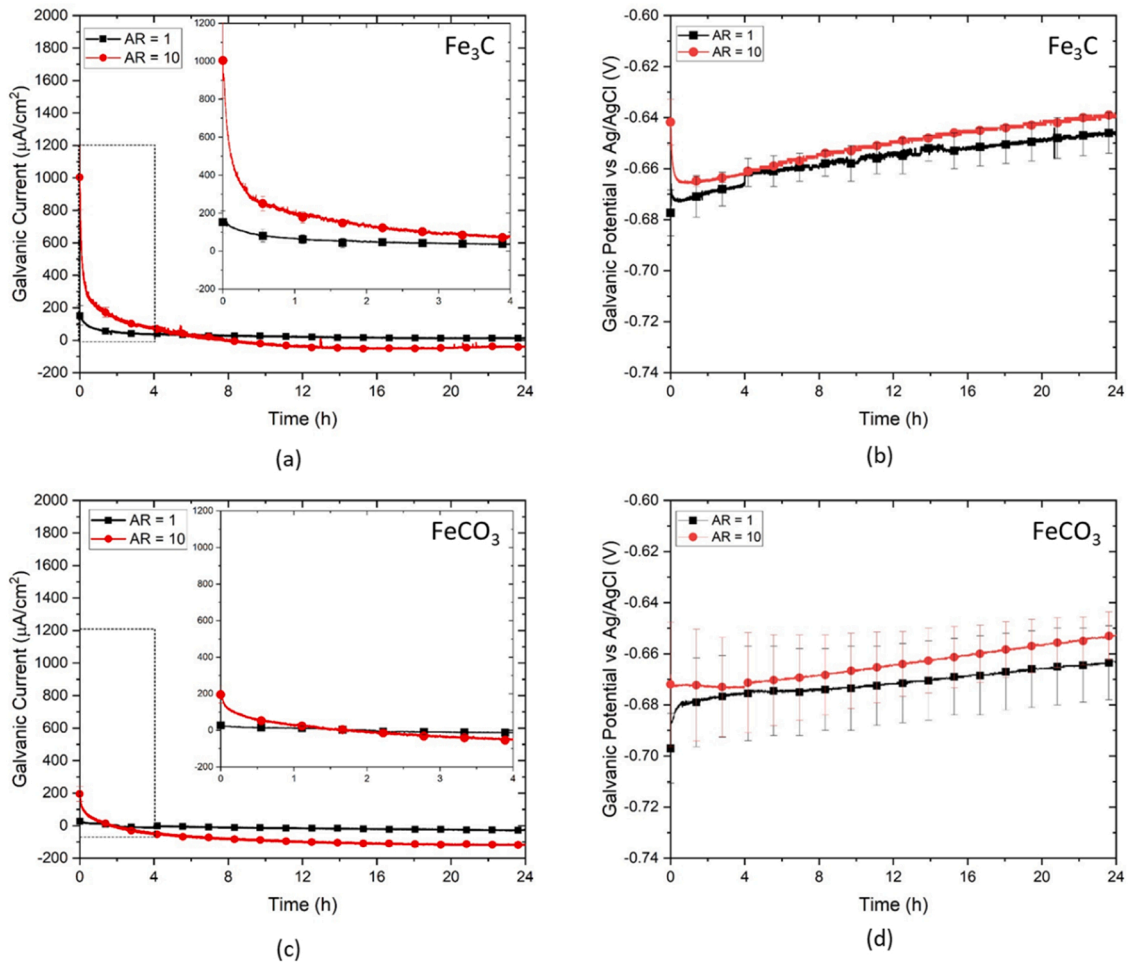

Fig. 7. (a, c) ZRA galvanic current and (b, d) galvanic potential measurements over 24 h at AR = 1:1 and AR = 10:1 in a CO_2-saturated, pH 5, 1 wt% NaCl solution at 50 °C obtained by coupling a wet ground X65 carbon steel coupon to (a, b) an Fe_3C-layered carbon steel coupon and (c, d) an $FeCO_3$-layered X65 carbon steel coupon. The dashed rectangle shows the area magnified in the inset plots.

was increased. A negative galvanic current (of approximately −35 μA/cm^2) was observed at the end of the test duration for an AR of 10:1, indicative of the net cathode and net anode switching polarity during the test. The enhanced revealing of Fe_3C on the bare steel may explain this.

Moving to the $FeCO_3$-bare X65 steel couple (Fig. 7(c)), no galvanic interaction was observed on the $FeCO_3$-bare steel couple for the AR of 1:1. However, a decrease in galvanic current during the first hour of the experiment was observed for the AR of 10:1. Over time, this galvanic current density dropped below 0 μA/cm^2 and ended at approximately − 120 μA/cm^2 after 24 h. This was indicative of the bare X65 steel coupon gradually becoming the net cathode. A similar switching was also observed at an AR 1:1 but at much lower currents (−27 μA/cm^2). Galvanic potentials increased during the experiment, in a similar manner to OCP increase at pH 5 in the absence of galvanic coupling (in the Supplementary Material), likely due to the revealing of Fe_3C on all coupons.

The significantly greater galvanic interaction caused by Fe_3C-layered coupons, compared to $FeCO_3$-layered coupon, can be clearly observed throughout the experiment, as expected with Fe_3C being a metallic conductor [29] and $FeCO_3$ an electrical insulator [22,23]. The average galvanic current of 319 μA/cm^2 measured during the first hour of the experiment at an AR of 10:1 for the Fe_3C-bare steel couple, was equivalent to a corrosion rate enhancement of approximately 3.7 mm/year. The gradual decrease in average galvanic current of the Fe_3C-bare X65 steel coupons to 0 μA/cm^2 is explained by the revealing of an Fe_3C network at the bare carbon steel coupon, observed in Fig. 5. The two coupons thus became similar in nature, both able to sustain cathodic and anodic reactions widely across the surface. Top-view SEM images and FIB-SEM cross section images of the Fe_3C-layered coupons and bare steel coupons after 4 h and 24 h galvanic corrosion experiments are shown in Figs. S7 and S8 in the Supplementary Material. All coupons (layered and bare steel) showed a clearly visible Fe_3C network on the surface, with no obviously identifiable characteristic differences between the layers.

For the $FeCO_3$-bare X65 carbon steel couple at an AR of 1:1, a very low galvanic current was measured. Top-view SEM images and FIB-SEM cross-sections of both $FeCO_3$-layered coupons and bare X65 carbon steel coupons after galvanic corrosion experiments are shown in Fig. 8 and Fig. 9, respectively. In Fig. 8(a) and (b), wide coverage of $FeCO_3$ is still observed on the layered surface after 4 h and 24 h of exposure, similar in appearance to the top-view SEM image of the layer after 24 h exposure in the pH 5 environment in the absence of a galvanic couple (Fig. 5(d)). On the bare carbon steel coupons (Fig. 8(c) and (d)), an Fe_3C network has been revealed. Fe_3C was also observed on cross-sections of both $FeCO_3$-layered coupons and bare X65 steel coupons, Fig. 9(a-d). Regions on the layered coupons between $FeCO_3$ crystals were analysed, showing a significant Fe_3C network had formed. Therefore, the lack of galvanic interaction is likely explained by the revealing of Fe_3C on both coupons.

At an AR of 10:1, however, the galvanic interaction was more significant. An initially positive galvanic current was observed in the first hour of the experiment, with the $FeCO_3$-layered coupon acting as the net cathode. Beyond 1 h, the average galvanic current decreased to approximately 0 μA/cm^2 for the $FeCO_3$-bare X65 steel couple over 4 h of

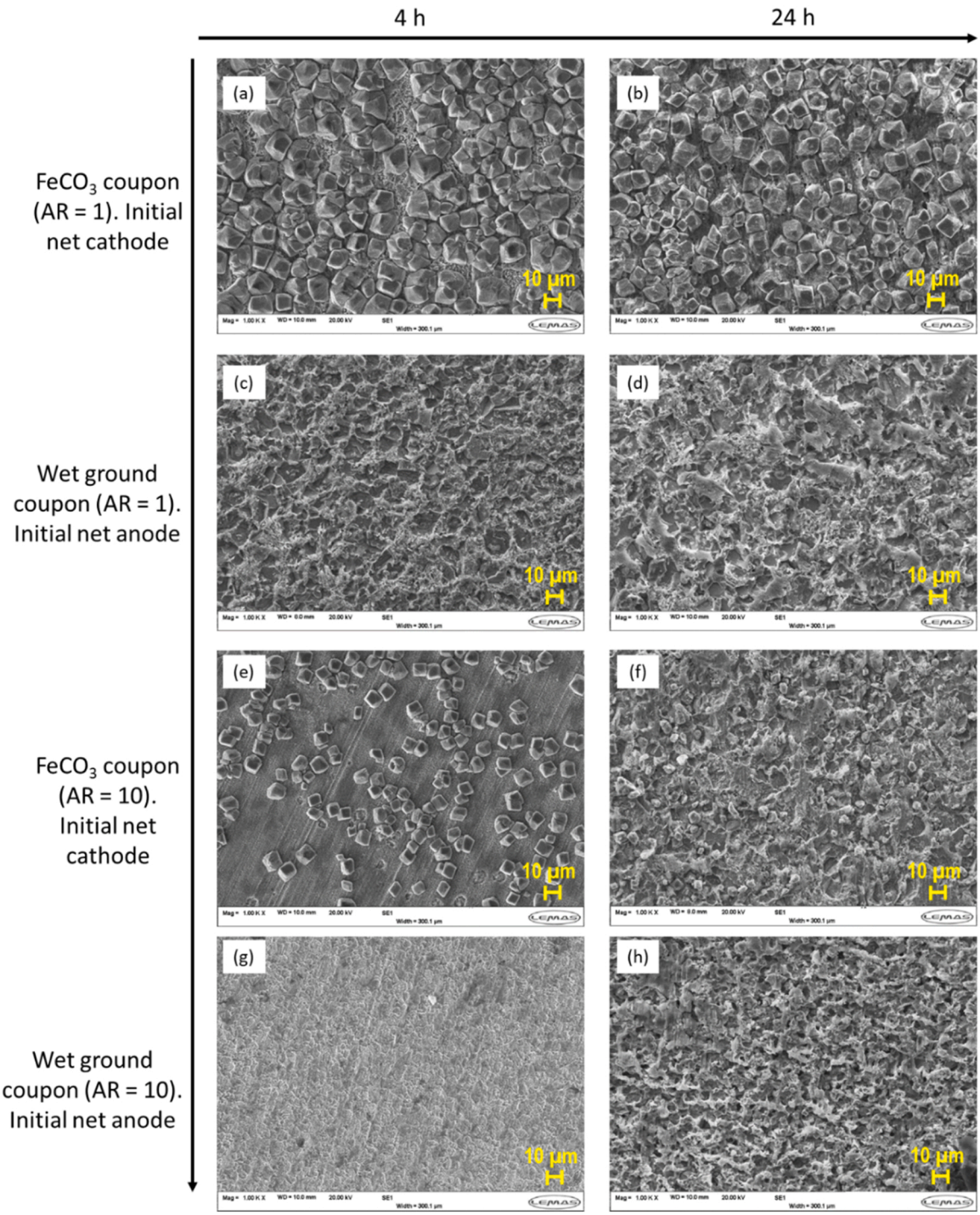

Fig. 8. SEM images of X65 carbon steel coupons after ZRA measurements performed at an AR of 1 (a-d) and AR = 10 (e-h) over 4 h (a, c, e and g) and 24 h (b, d, f and h) in a CO_2-saturated, pH 5, 1 wt% NaCl solution at 50 °C by coupling a wet ground X65 carbon steel coupon to an $FeCO_3$-layered X65 carbon steel coupon.

exposure. However, as observed in Fig. 7(c), the actual galvanic current had decreased below 0 μA/cm^2 by this stage and was measured to be approximately − 50 μA/cm^2. Therefore, the bare X65 steel coupon had become a net cathode, with the $FeCO_3$-layered coupon acting as the net anode within 4 h of exposure. This trend continued until the end of the 24 h period with the magnitude of the galvanic current increasing to − 120 μA/cm^2. An Fe_3C network was again revealed on the surface of the bare carbon steel coupons, shown in top view SEM images and FIB-SEM images in Fig. 8(g) and (h) and Fig. 9(g) and (h). However, at an AR of 10:1, it was observed on top-view SEM images in Fig. 8(e) and (f) that $FeCO_3$ coverage was significantly reduced on the carbon steel surface. When comparing to Fig. 5(d), it becomes clear that the galvanic interaction played a significant role in the $FeCO_3$ layer removal. The authors suggest that the cause of the reversal of the galvanic current was due to the revealing of the Fe_3C network on the bare X65 carbon steel coupon, which was accelerated during the first hour of the experiment due to galvanic interaction enhancing the corrosion rate of the bare steel coupon. This layer was then able to sustain the cathodic reaction, thus becoming the net cathode and enhancing the corrosion rate of the $FeCO_3$-layered coupon. As the $FeCO_3$-layered coupon gradually transitioned to showing net anode behaviour (sustaining the anodic dissolution of iron reaction on the bare steel, Eq. (2)), it is logical that pH local

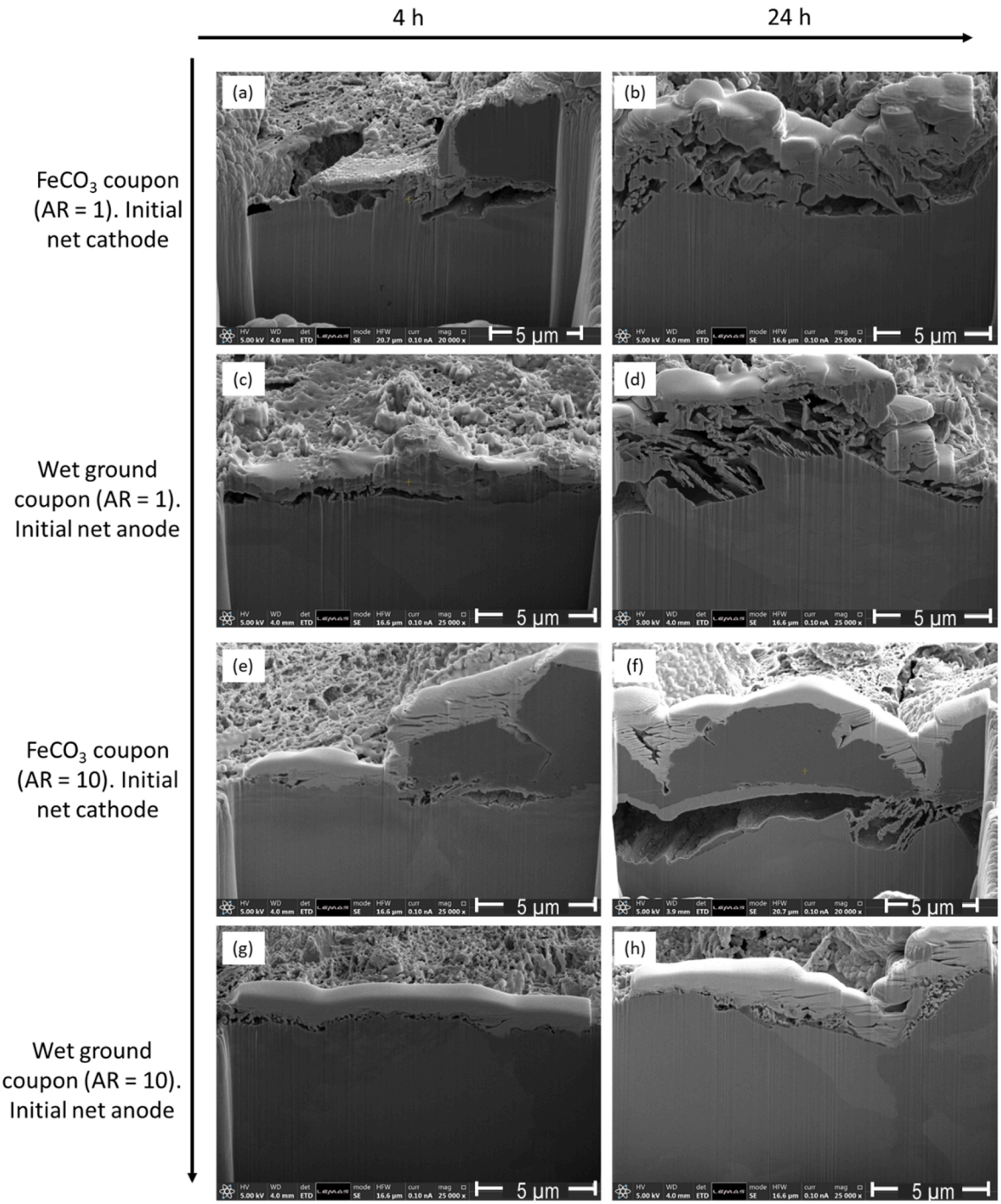

Fig. 9. SEM images obtained after FIB milling to show a cross section of the surface layers formed after ZRA measurements performed at an AR = 1 (a-d) and AR = 10 (e-h) over 4 h (a, c, e and g) and 24 h (b, d, f and h) in a CO_2-saturated, pH 5, 1 wt% NaCl solution at 50 °C by coupling a wet ground X65 carbon steel coupon to an $FeCO_3$-layered X65 carbon steel coupon.

to the coupon surface is lower than a coupon showing net cathode behaviour [25]. This, therefore, promotes Eq. (5) and the dissolution of the $FeCO_3$ layers.

3.4. Potentiodynamic polarisation after galvanic corrosion experiments (Method IV)

The relevance of these findings was evaluated by potentiodynamic polarisation measurements carried out after 4 h and 24 h of galvanic interaction on both the layered and bare X65 steel coupons. Coupons were no longer galvanically coupled and OCP was allowed to stabilise for 5 min prior to starting the measurements shown in Fig. 10. For the Fe_3C-bare X65 steel couples, no significant difference in OCP was observed between the Fe_3C-layered coupon and corresponding bare X65 steel coupon, explaining the relatively small galvanic current measured in Fig. 7 between 4 h and 24 h. Cathodic current density plateaus were higher for the Fe_3C-exposed electrodes and after 24 h compared to the bare steel. Higher corrosion current densities were observed on the AR of 10:1 electrodes, Fig. 10(b), showing how the increased galvanic current at this area ratio resulted in higher rates of general corrosion. Higher anodic current densities were also observed on the bare steel coupons in Fig. 10(b) due to the enhanced corrosion of this layer and

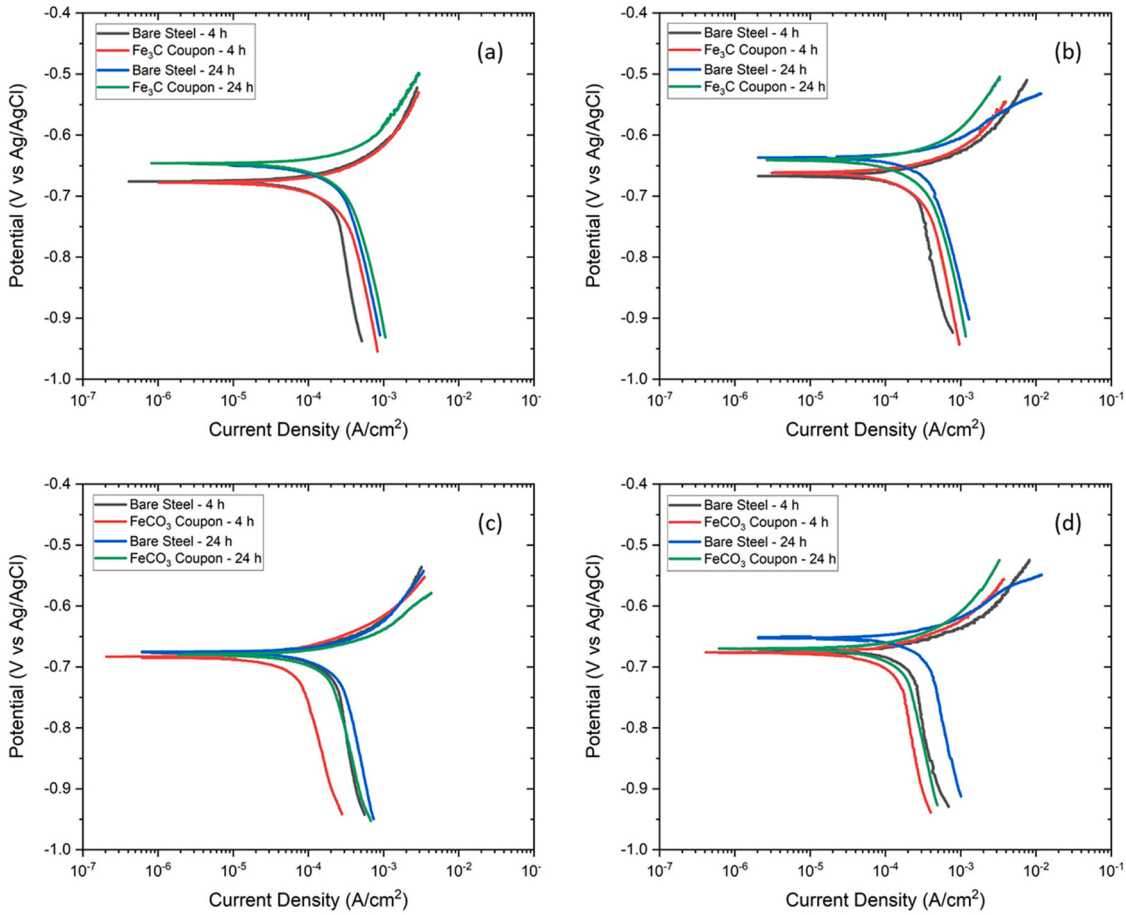

Fig. 10. Potentiodynamic polarisation plots of bare X65 carbon steel and layered X65 carbon steel coupons measured after 4 h and 24 h galvanic corrosion experiments in a pH 5, CO_2-saturated, 1 wt% NaCl solution at 50 °C for an (a) Fe_3C-bare steel couple at AR = 1, (b) Fe_3C-bare steel couple at AR = 10, (c) $FeCO_3$-bare steel couple at AR = 1 and (d) $FeCO_3$-bare steel couple at AR = 10.

formation of Fe_3C.

Potentiodynamic polarisation of the coupons after the $FeCO_3$-bare steel galvanic couple experiments, Fig. 10(c) and (d), showed that the protectiveness of the $FeCO_3$ layer was reduced over time, because of galvanic interaction. Corrosion current densities for all coupons were higher on the AR = 10 coupons, Fig. 10(d), compared to AR = 1 coupons. Like the Fe_3C-layered coupons, the difference in OCP was not significant between the $FeCO_3$-layered coupons and bare X65 steel coupons. However, at an AR of 10:1 after 24 h, the bare X65 steel took up the role as the net cathode (see more noble OCP in Fig. 11(d)) and the $FeCO_3$-layered coupon became the net anode.

3.5. Galvanic corrosion experiments with pure iron (Method IV)

To confirm the hypothesis that the revealing of Fe_3C on the bare X65 carbon steel coupon resulted in the reversal of the galvanic current and enhanced the corrosion rate of the $FeCO_3$-layered coupon, galvanic corrosion experiments using $FeCO_3$-layered coupons (*initial* cathode) were repeated and coupled to a pure iron coupon instead of X65 carbon steel, at an AR of 10. These experiments, therefore, prevent the gradual revealing of Fe_3C on the *initial* net anode pure iron (as there is no carbon phase present in the microstructure). The measured galvanic currents and galvanic potential for pure iron are compared with the results for the $FeCO_3$-bare carbon steel couple in Fig. 11. When coupled to pure iron, the galvanic current remained positive and greater than 100 μA/cm^2 throughout the 24 h period, a significant difference compared to the $FeCO_3$-bare X65 steel couple. These results clearly confirmed the hypothesis that the revealing of the Fe_3C network on the *initial* anode bare carbon steel surface was key to reversing the galvanic current and enhancing the corrosion rate of the $FeCO_3$-layered coupon.

SEM analysis of the coupons after 24 h of the $FeCO_3$-pure iron couple showed that significant surface coverage of $FeCO_3$ remained, which was not the case when coupled to bare X65 carbon steel. As the $FeCO_3$-layered coupon remains as the net cathode when coupled to pure iron, it is likely that pH local to the $FeCO_3$-layered coupon surface is higher than the net anode, maintaining conditions more favourable for the survival of $FeCO_3$ [24,25]. A higher resolution image (Fig. 12(c)) and a cross-section of the $FeCO_3$ layer (Fig. 12(d)) after 24 h of galvanic interaction with pure iron are also shown. The presence of Fe_3C on the carbon steel suggests that this is the most likely cause of galvanic interaction, as opposed to the insulating $FeCO_3$. Results obtained in similar conditions (1 wt% NaCl, CO_2-saturated solution at pH 6 and 60 °C) by galvanically coupling a pure iron coupon layered with $FeCO_3$ crystals to a bare pure iron coupon showed galvanic currents of approximately 1 μA/cm^2 (at an equal area ratio), several orders of magnitude lower than Fig. 11, suggesting Fe_3C plays a major role in the galvanic interaction observed [27]. A greater difference in OCP was observed between $FeCO_3$ and pure iron in Fig. 6, thus explaining the slightly more negative mixed potential measured in Fig. 11 for the pure iron-$FeCO_3$ couple.

3.6. Significance of galvanic corrosion caused by surface layers

The results in Fig. 11 demonstrate how critical the presence of Fe_3C on a surface is for driving galvanic interaction. The dominance of Fe_3C in galvanic corrosion compared to $FeCO_3$ is clear, with the galvanic

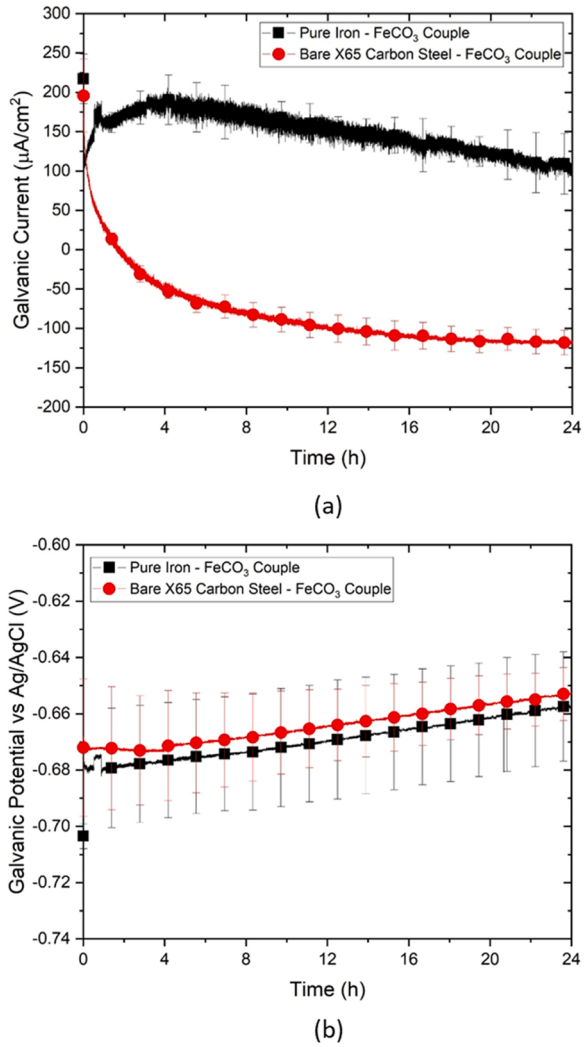

Fig. 11. Comparison of galvanic current and galvanic potential measurements in a CO_2-saturated, pH 5, 1 wt% NaCl solution at 50 °C for a wet ground pure iron coupon coupled to an $FeCO_3$-layered coupon and wet ground X65 carbon steel coupled to an $FeCO_3$-layered coupon at AR = 10:1.

interaction initiated by Fe_3C able to contribute to the removal of $FeCO_3$ in the pH 5, CO_2-saturated saturated solution and create a significant galvanic interaction with bare carbon steel. Due to the more conductive nature of Fe_3C, it is therefore suggested by the authors that galvanic corrosion is predominantly driven by the presence of Fe_3C on the carbon steel surface, something widely reported in literature [1,9,11,12,33] and observed in this study, e.g. Fig. 8, Fig. 9 and Fig. 12, as opposed to being caused by $FeCO_3$. The insulating nature of $FeCO_3$ [23] and evidence of the blocking of actively corroding sites by $FeCO_3$ [5,6,37], offers further evidence. The dissolution of $FeCO_3$ is also likely promoted as a result of the net cathodic behaviour of Fe_3C relative to carbon steel and $FeCO_3$ and the influence this would have on local pH. A lower interfacial pH on a $FeCO_3$-layered coupon acting as net anode would likely enhance $FeCO_3$ dissolution, as opposed to a $FeCO_3$-layered coupon acting as net cathode, as observed in Fig. 11. Unavoidable dissolution of $FeCO_3$ in the pH 5 conditions was observed, however, SEM images showed extensive $FeCO_3$ coverage on the surface in the absence of galvanic corrosion (Fig. 5) and after a galvanic couple with pure iron (Fig. 12). Therefore, galvanic coupling to bare carbon steel played a significant role in enhancing the $FeCO_3$ layer dissolution.

The general decreasing trend in galvanic current for layered coupons coupled to bare carbon steel shown in Fig. 7, and observed in studies by Barker et al. [2], Han et al. [19] and Fernandez et al. [21] for $FeCO_3$-bare steel couples, is potentially explained by the revealing of Fe_3C on bare carbon steel surfaces (or the development of another conductive layer, such as magnetite [27,35]). The revealing of Fe_3C would increase the OCP of the bare steel coupon, minimising the OCP difference and galvanic interaction between the layered and bare coupons. This decrease in galvanic current was not observed, for example, with an $FeCO_3$-pure iron couple in Fig. 11, as the absence of Fe_3C on the pure Fe coupon maintained a clear distinction between the net cathode and net anode coupons.

Studying galvanic interaction between surface layers and bare steel is challenging due to the highly localised nature of the galvanic cells that form, the variation in $FeCO_3$ characteristics and the likely changes in solution chemistry local to a surface. It was very difficult to demonstrate the significance of changes in the localised chemistry underneath, or local to the $FeCO_3$ crystals [6] using the methodologies reported in this study, but this could have potentially accounted for some proportion of the galvanic current measured between $FeCO_3$-layered coupons and bare steel or pure iron. Therefore, accounting for all variables is not possible, such as the influence of microstructure or alloy composition on $FeCO_3$ [8,42], influence of $FeCO_3$ crystal size [5], presence of other layers (e.g. magnetite) [36] or attempting to replicate supersaturated conditions [10]. At 50 °C and pH 5, i.e. conditions below the saturation point of $FeCO_3$, dissolution of $FeCO_3$ is expected, although this study showed that galvanic interaction with Fe_3C can exacerbate it. Another potential reason for the mechanisms of removal of $FeCO_3$ is due to the more realistic AR studied. Numerous EIS studies have shown that surface coverage by $FeCO_3$ is significantly lower than microscopy analyses or corrosion rates, determined from LPR measurements, often imply. Therefore, ARs reported in literature of > >10:1 represent a more significant net cathode to net anode proportion than would be realistic of partial layer coverage seen in practice. The ARs studied allowed for a more realistic bare steel surface area for an Fe_3C network to form, with greater surface coverage of Fe_3C expected to play a more significant role in galvanic corrosion [11].

4. Conclusions

Galvanic interaction of Fe_3C and $FeCO_3$ surface layers formed on carbon steel in a pH 5, 1 wt% NaCl, CO_2-saturated solution at a temperature of 50 °C was evaluated at two different ARs of 1:1 and 10:1 to establish an understanding of galvanic corrosion. The main findings from the study were:

- The galvanic interaction caused by an Fe_3C-layered coupon was far greater than the galvanic interaction caused by an $FeCO_3$-layered coupon, with galvanic currents over 4 h averaging 169 μA/cm^2 and 4 μA/cm^2, respectively, for ARs of 10:1
- As expected, galvanic interaction was more significant at an AR of 10:1, compared to 1:1, realistic ARs that represent partial coverage of $FeCO_3$ on a carbon steel surface
- Galvanic interaction was reversed at an AR of 10:1 between an $FeCO_3$-layered coupon and bare X65 carbon steel after 24 h of galvanic corrosion, due to the revealing of an Fe_3C network on the bare steel coupon causing it to become the net cathode
- The revealing of Fe_3C on the initial net anode coupon caused the removal of $FeCO_3$ crystals on the initial net cathode coupon, likely due to the interfacial acidification resulting from the enhanced corrosion of the $FeCO_3$-layered electrode
- Coupling of the $FeCO_3$-layered coupon to a pure iron coupon at an AR of 10:1 showed no significant decrease in galvanic current, confirming the hypothesis that the revealing of Fe_3C on the bare steel anode enhanced degradation of the $FeCO_3$-layered coupon
- The high conductivity Fe_3C and its ability to enhance degradation of an $FeCO_3$-layered coupon suggests that the cause of galvanic

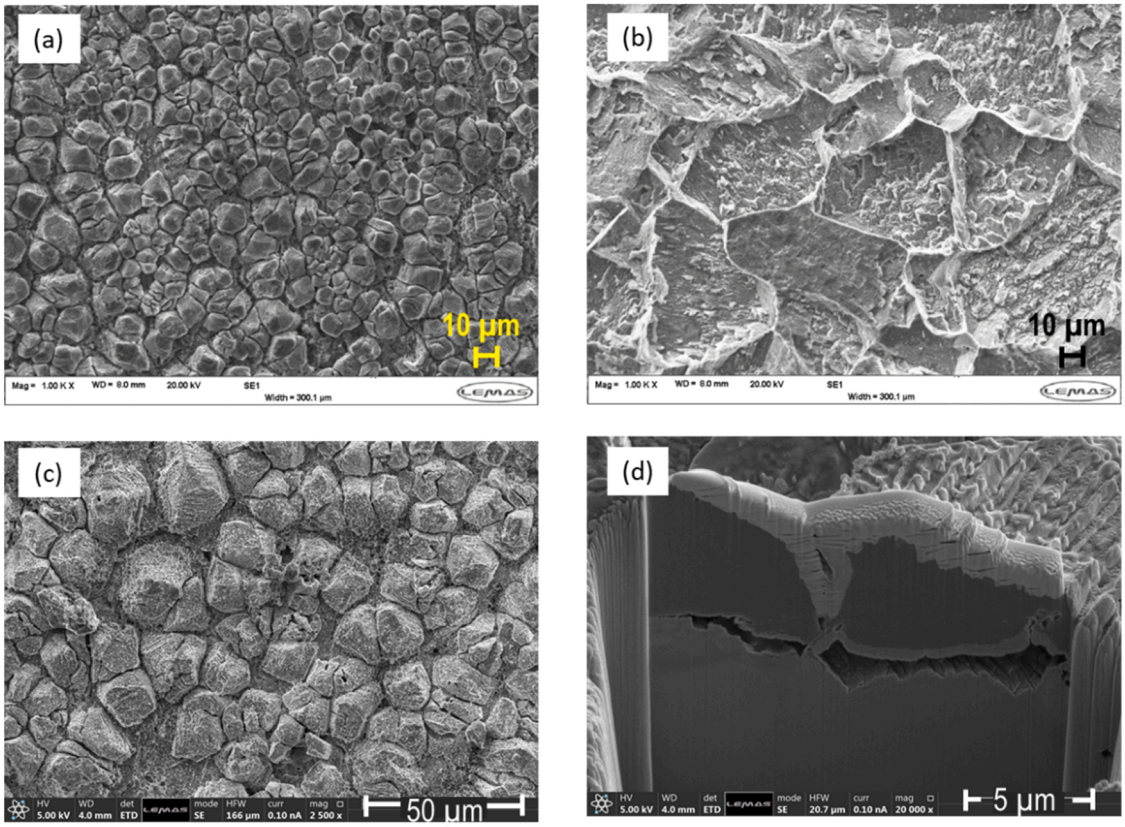

Fig. 12. SEM and FIB-SEM images obtained after galvanic corrosion measurements in a CO_2-saturated, pH 5, 1 wt% NaCl solution at 50 °C for a galvanic couple consisting of (a) an $FeCO_3$-layered X65 carbon steel coupon, (b) a pure iron coupon at AR = 10, (c) a high resolution SEM image of an $FeCO_3$-layered X65 carbon steel coupon and (d) a cross-section of the $FeCO_3$-layered X65 carbon steel coupon.

interaction for $FeCO_3$-layered coupons is due to the presence of Fe_3C within the $FeCO_3$ layer.

CRediT authorship contribution statement

Joshua Owen: Conceptualisation, Methodology, Investigation, Formal analysis, Writing – original draft, Funding acquisition. **Francois Ropital:** Methodology, Supervision, Writing – review & editing, Funding acquisition. **Gaurav Joshi:** Methodology, Supervision, Writing – review & editing. **Jean Kiteel:** Methodology, Supervision, Resources, Writing – review & editing. **Richard Barker:** Supervision, Conceptualisation, Methodology, Writing – review & editing, Funding acquisition.

Declaration of Competing Interest

The authors declare that they have no known competing financial interests or personal relationships that could have appeared to influence the work reported in this paper.

Data Availability

The raw/processed data required to reproduce these findings cannot be shared at this time as the data also forms part of an ongoing study.

Acknowledgements

The authors would like to acknowledge funding from Engineering and Physical Sciences Research Council (grant number: EP/T009160/1) and the Royal Society (grant number: IES\R1\211068). The authors would also like to thank the contribution from John Harrington at University of Leeds Electron Microscopy and Spectroscopy Centre (LEMAS) for completion of SEM and FIB-SEM imaging.

Appendix A. Supporting information

Supplementary data associated with this article can be found in the online version at doi:10.1016/j.corsci.2022.110762.

References

[1] R. Barker, D. Burkle, T. Charpentier, H. Thompson, A. Neville, A review of iron carbonate ($FeCO_3$) formation in the oil and gas industry, Corros. Sci. 142 (2018) 312–341.
[2] R. Barker, R. Yazdi, Y. Hua, A. Jackson, A. Ghanbarzadeh, M. Huggan, T. Charpentier, A. Neville, Development of an automated underwater abrasion rig to determine galvanic effects during the growth and localised breakdown of surface films in CO_2-containing solutions, Rev. Sci. Instrum. 90 (3) (2019), 034101.
[3] D. Burkle, R. De Motte, W. Taleb, A. Kleppe, T. Comyn, S. Vargas, A. Neville, R. Barker, In situ SR-XRD study of $FeCO_3$ precipitation kinetics onto carbon steel in CO_2-containing environments: the influence of brine pH, Electrochim. Acta 255 (2017) 127–144.
[4] R. De Motte, R. Barker, D. Burkle, S. Vargas, A. Neville, The early stages of $FeCO_3$ scale formation kinetics in CO_2 corrosion, Mater. Chem. Phys. 216 (2018) 102–111.
[5] R. De Motte, E. Basilico, R. Mingant, J. Kittel, F. Ropital, P. Combrade, S. Necib, V. Deydier, D. Crusset, S. Marcelin, A study by electrochemical impedance spectroscopy and surface analysis of corrosion product layers formed during CO_2 corrosion of low alloy steel, Corros. Sci. 172 (2020), 108666.
[6] A. Lazareva, J. Owen, S. Vargas, R. Barker, A. Neville, Investigation of the evolution of an iron carbonate layer and its effect on localized corrosion of X65 carbon steel in CO_2 corrosion environments, Corros. Sci. 192 (2021), 109849.
[7] E.V. Senatore, W. Taleb, J. Owen, Y. Hua, J.A.C.P. Gomes, R. Barker, A. Neville, Evaluation of high shear inhibitor performance in CO_2-containing flow-induced corrosion and erosion-corrosion environments in the presence and absence of iron carbonate films, Wear 404–405 (2018) 143–152.
[8] Berntsen, T., Seiersten, M., Hemmingsen, T. Effect of $FeCO_3$ supersaturation and carbide exposure on the CO_2 corrosion rate of carbon steel. in CORROSION 2011. 2011. Houston, TX, USA.

[9] M. Gao, X. Pang, K. Gao, The growth mechanism of CO_2 corrosion product films, Corros. Sci. 53 (2) (2011) 557–568.
[10] W. Sun, S. Nešic, Kinetics of corrosion layer formation: part 1 - iron carbonate layers in carbon dioxide corrosion, CORROSION 64 (4) (2008) 334–346.
[11] F. Farelas, M. Galicia, B. Brown, S. Nesic, H. Castaneda, Evolution of dissolution processes at the interface of carbon steel corroding in a CO_2 environment studied by EIS, Corros. Sci. 52 (2) (2010) 509–517.
[12] J. Crolet, N. Thevenot, S. Nesic, Role of conductive corrosion products in the protectiveness of corrosion layers, Corrosion 54 (3) (1998) 194–203.
[13] H. Bhadeshia, Cementite, J. Int. Mater. Rev. 65 (1) (2020) 1–27.
[14] M.-C. Lee, G. Simkovich, Electrical conduction behavior of cementite, Fe3C, Metall. Trans. A 18 (3) (1987) 485–486.
[15] Owen, J., Ropital, F., Joshi, G., Kittel, J., Barker, R. Galvanic Interactions between Surface Layers and Bare Carbon Steel in Aqueous CO_2 Environments. in AMPP Annual Conference + Expo. 2022. San Antonio, TX, USA: AMPP.
[16] S. Nesic, N. Thevenot, J.-L. Crolet, D. Drazic, Electrochemical properties of iron dissolution in the presence of CO_2 - basics revisited. CORROSION 96, NACE International, Houston, TX, USA, 1996.
[17] K. Videm, A. Dugstad, Corrosion of carbon steel in an aqueous carbon dioxide environment Part 1, Mater. Perform. 28 (3) (1989).
[18] K. Videm, J. Kvarekval, T.E. Perez, G. Fitzsimons, Surface effects on the electrochemistry of iron and carbon steel electrodes in aqueous CO_2 solutions. CORROSION 96, NACE International, Denver, CO, USA, 1996.
[19] J. Han, B. Brown, S. Nešic, Investigation of the galvanic mechanism for localized carbon dioxide corrosion propagation using the artificial pit technique, Corrosion 66 (9) (2010) 095003–095003-12.
[20] J.R. Shadley, S.A. Shirazi, E. Dayalan, M. Ismail, E.F. Rybicki, Erosion-corrosion of a carbon steel elbow in a carbon dioxide environment, Corrosion 52 (9) (1996) 714–723.
[21] R.M. Fernández-Domene, R. Leiva-García, J. Andrews, R. Akid, Galvanic corrosion following local breakdown of a scale formed on X-65 in CO_2 saturated solutions. CORROSION, NACE International,, Dallas, TX, USA, 2015.
[22] F. Mercier-Bion, J. Li, H. Lotz, L. Tortech, D. Neff, P. Dillmann, Electrical properties of iron corrosion layers formed in anoxic environments at the nanometer scale, Corros. Sci. 137 (2018) 98–110.
[23] G.A. Schmitt, M. Mueller, M. Papenfuss, E. Strobel-Effertz, Understanding localized CO_2 corrosion of carbon steel from physical properties of iron carbonate scales. CORROSION 99, NACE International, San Antonio, TX, 1999.
[24] R. De Motte, R. Mingant, J. Kittel, F. Ropital, P. Combrade, S. Necib, V. Deydier, D. Crusset, Near surface pH measurements in aqueous CO_2 corrosion, Electrochim. Acta 290 (2018) 605–615.
[25] J. Han, B.N. Brown, D. Young, S. Nešić, Mesh-capped probe design for direct pH measurements at an actively corroding metal surface, J. Appl. Electrochem. 40 (3) (2010) 683–690.
[26] E. Basilico, S. Marcelin, R. Mingant, J. Kittel, M. Fregonese, R. Barker, J. Owen, A. Neville, F. Ropital, Effect of O_2 contamination on carbon steel pseudo-passive scales in CO_2 aqueous solutions, Corros. Sci. 205 (2022), 110388.
[27] A.H. Gonzalez, G. Frankel, J. Vera, W. Durnie, R. Woollam, Galvanic interactions between Fe electrodes in CO_2-saturated solutions with different pH, Corrosion 77 (11) (2021) 1203–1217.
[28] N. Ochoa, C. Vega, N. Pébère, J. Lacaze, J.L. Brito, CO_2 corrosion resistance of carbon steel in relation with microstructure changes, Mater. Chem. Phys. 156 (2015) 198–205.
[29] D. Staicopolus, The role of cementite in the acidic corrosion of steel, J. Electrochem. Soc. 110 (11) (1963) 1121.
[30] J. Owen, J. Godfrey, W. Ma, G. de Boer, M. Al-Khateeb, H. Thompson, A. Neville, C. Ramsey, R. Barker, An experimental and numerical investigation of CO_2 corrosion in a rapid expansion pipe geometry, Corros. Sci. 165 (2020), 108362.
[31] A. Matamoros-Veloza, R. Barker, S. Vargas, A. Neville, Mechanistic insights of dissolution and mechanical breakdown of $FeCO_3$ corrosion films, ACS Appl. Mater. Interfaces 13 (4) (2021) 5741–5751.
[32] Y. Hua, S. Xu, Y. Wang, W. Taleb, J. Sun, L. Zhang, R. Barker, A. Neville, The formation of $FeCO_3$ and Fe_3O_4 on carbon steel and their protective capabilities against CO_2 corrosion at elevated temperature and pressure, Corros. Sci. 157 (2019) 392–405.
[33] E. Basilico, S. Marcelin, R. Mingant, J. Kittel, M. Fregonese, F. Ropital, The effect of chemical species on the electrochemical reactions and corrosion product layer of carbon steel in CO_2 aqueous environment: a review, Mater. Corros. 72 (2021) 1152–1167.
[34] M. Ko, B. Ingham, N. Laycock, D.E. Williams, In situ synchrotron X-ray diffraction study of the effect of microstructure and boundary layer conditions on CO_2 corrosion of pipeline steels, Corros. Sci. 90 (2015) 192–201.
[35] G.D. Song, S.-H. Jeon, Y.-H. Son, J.G. Kim, D.H. Hur, Galvanic effect of magnetite on the corrosion behavior of carbon steel in deaerated alkaline solutions under flowing conditions, Corros. Sci. 131 (2018) 71–80.
[36] J. Han, D. Young, H. Colijn, A. Tripathi, S. Nešić, Chemistry and structure of the passive film on mild steel in CO_2 corrosion environments, Ind. Eng. Chem. Res. 48 (13) (2009) 6296–6302.
[37] M. Al Kindi, G.R. Joshi, K. Cooper, J. Andrews, P. Arellanes-Lozada, R. Leiva-Garcia, D.L. Engelberg, O. Bikondoa, R. Lindsay, Substrate protection with corrosion scales: can we depend on iron carbonate? ACS Appl. Mater. Interfaces (2021).
[38] G.R. Joshi, K. Cooper, X. Zhong, A.B. Cook, E.A. Ahmad, N.M. Harrison, D. L. Engelberg, R. Lindsay, Temporal evolution of sweet oilfield corrosion scale: Phases, morphologies, habits, and protection, Corros. Sci. 142 (2018) 110–118.
[39] B. Kinsella, Y. Tan, S. Bailey, Electrochemical impedance spectroscopy and surface characterization techniques to study carbon dioxide corrosion product scales, Corrosion 54 (10) (1998) 835–842.
[40] D. Lopez, Wd Schreiner, S. De Sánchez, S. Simison, The influence of carbon steel microstructure on corrosion layers: an XPS and SEM characterization, Appl. Surf. Sci. 207 (1–4) (2003) 69–85.
[41] A. Matamoros-Veloza, R. Barker, S. Vargas, A. Neville, Iron calcium carbonate instability: structural modification of siderite corrosion films, ACS Appl. Mater. Interfaces 12 (43) (2020) 49237–49244.
[42] S. Al-Hassan, B. Mishra, D. Olson, M. Salama, Effect of microstructure on corrosion of steels in aqueous solutions containing carbon dioxide, Corrosion 54 (06) (1998) 480–491.